Compact see-through near-eye display with depth adaption

Yun-Han Lee (SID Student Member)
Guanjun Tan (SID Student Member)
Kun Yin (SID Student Member)
Tao Zhan
Shin-Tson Wu (SID Fellow)

Abstract — Based on the recent development of Pancharatnam–Berry deflectors and lenses, we propose a compact and lightweight near-eye display system with depth adaption. The compact design results from the polarization selectivity of Pancharatnam–Berry deflector waveguide coupler, and the fast-switching Pancharatnam–Berry lenses can be exploited for generating correct light fields.

Keywords — *augmented reality, wearable display, near-eye display system.*

DOI # 10.1002/jsid.635

1 Introduction

The objective of this paper is to develop a compact and lightweight optical system for augmented reality displays[1,2] with depth information using Pancharatnam–Berry optical elements as a deflector (PBD) or as a lens (PBL).[3–8] Our approach promises a more compact design and better functionality for the near-eye displays.

The Pancharatnam–Berry optical elements can be analyzed as a patterned half-wave plate. The Jones matrix representation of a circularly polarized input can be described as

$$\begin{bmatrix} \cos 2\phi & \sin 2\phi \\ \sin 2\phi & -\cos 2\phi \end{bmatrix} \begin{bmatrix} 1 \\ \pm i \end{bmatrix} = \begin{bmatrix} 1 \\ \mp i \end{bmatrix} e^{\pm 2i\phi}, \tag{1}$$

where ϕ denotes the azimuthal axis angle of the half-wave plate. From Eq. (1), it is obvious that the half-wave plate does not only reverse the chirality of the input light but also introduce a wavefront delay, depending on the azimuthal axis of the half-wave plate. This "decoding" of azimuthal axis distribution to the wavefront phase delay, also known as geometric phase, can be exploited for thin and high-efficiency optical elements. Depending on the desired output wavefront, the Pancharatnam–Berry optical elements can be made into lenses (parabolic wavefront) or deflectors (linear wavefront). As reported in Oh and Escuti,[5] a diffraction efficiency over 98% at normal incidence can be achieved in the entire visible spectrum. On the contrary, the encoding process of geometric phase requires the interference of two circularly polarized beams with opposite chirality. This can also be presented through Jones matrix as

$$\begin{bmatrix} 1 \\ i \end{bmatrix} e^{-i\theta} + \begin{bmatrix} 1 \\ -i \end{bmatrix} e^{i\theta} = 2 \begin{bmatrix} \cos\theta \\ \sin\theta \end{bmatrix}, \tag{2}$$

where θ here represents the wavefront delay of the input light. As shown in Eq. (2), a total wavefront delay of 2θ (between left-handed and right-handed circularly polarized light) maps to a linearly polarized light with an azimuthal angle θ.

A reflective PBD can be regarded as a polarization-selective holographic grating.[7] The liquid crystal orientation in a PBD forms a Bragg grating (Fig. 1(a)). Let us assume the left-handed circularly polarized light is deflected (Fig. 1(b)), then the right-handed circularly polarized light will pass through at almost 100% efficiency (Fig. 1(c)). This type of deflection grating couplers has flexible selection of index contrast due to the wide versatility of liquid crystal polymer materials.

On the other hand, a transmissive PBL is essentially a patterned half-wave plate (Fig. 2(a)) with encoded parabolic phase profile.[8] A PBL can focus or defocus the light, depending on the handedness of the input circularly polarized light. Therefore, by combining PBLs with polarization rotators, the focusing power can be electrically switched between two focal lengths: $+f_0$ and $-f_0$ (on-state and off-state). It is straightforward to add a refractive lens to offset the focusing power to desired values. In Fig. 2(b), we show the switching of PBL placed in adjacent of a refractive lens so that the optical power is positive in both on-state and off-state. It can be seen that the distance of the magnified words shifts from 12.5 to 350 cm simply by applying a voltage. A large change in optical power can be achieved, and yet for depth adaption in near-eye displays, a change of three diopters is usually sufficient. Such switching has a response time of 1 ms. By stacking N pieces of PBLs with polarization rotators, we can achieve 2^N switchable states. In this case, the polarization of the light must be carefully analyzed to prevent possible ghost image from the PBL. An example of a stacked PBL is shown in Fig. 2(c). A polarizer (P) is placed at the input side to ensure well-defined polarization state. Three twisted nematic (TN) liquid crystal cells are used as polarization rotators for the linearly polarized light. To ensure high efficiency, the linearly polarized light needs to be converted to circularly polarized light as it enters PBLs. Therefore, the three PBLs are

Received 02/17/18; accepted 03/01/18.
The authors are with the College of Optics and Photonics, University of Central Florida, Orlando, FL 32816, USA; e-mail: swu@creol.ucf.edu.
© Copyright 2018 Society for Information Display 1071-0922/18/2602-0635$1.00.

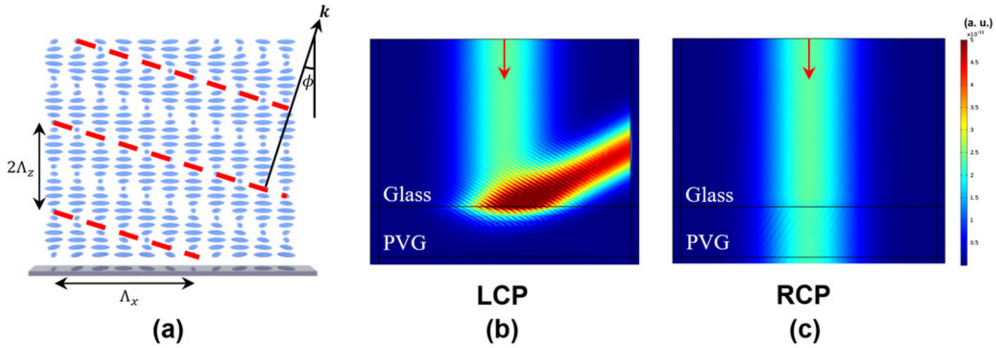

FIGURE 1 — (a) The molecular director variation in x–z plane (translational symmetric along y-axis). (b) The left-handed circularly polarized (LCP) input (from top) is deflected toward the right, and (c) the right-handed circularly polarized (RCP) input is not deflected.

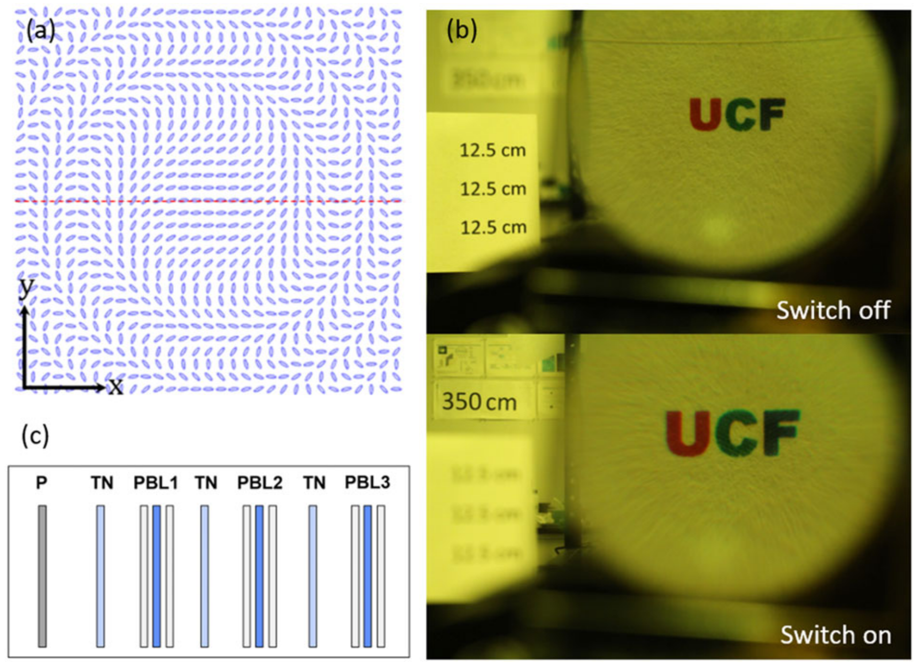

FIGURE 2 — (a) Liquid crystal director orientation in the x–y plane. (b) An example of switching Pancharatnam–Berry lens (PBL). (c) Illustration of a stacked PBL with eight switchable focal lengths. White blocks are quarter-wave films. P, polarizer; TN, twisted nematic.

sandwiched by broadband quarter-wave plates (white blocks). By placing three sets of TN-PBL in sequence, switching of eight focal lengths can be achieved.

2 Fabrication of Pancharatnam–Berry phase lens and deflector

The encoding of Pancharatnam–Berry phase lens and deflector can be realized by interference exposure.[9] The glass substrate was first prepared by spin-coating photo-alignment material such as Brilliant Yellow azo-dye.[10] The coated substrate was then placed onto the polarized Mach–Zehnder interferometer as Fig. 3 depicts. In this optical setup, a linearly polarized blue/ultraviolet (UV) laser source was first filtered with a microscope objective (O) and a pin-hole (P). The filtered beam was collimated with a lens (L) and passing through a non-polarizing beam splitter to split the beam into recording and reference beams. Each of these two beams was reflected by a mirror (M), passing through a quarter-wave plate and then being converted to circularly polarized light with opposite chirality. To generate linear wavefront, the recording beam is tilted to induce linear delay with respect to the reference beam. To generate parabolic wavefront, a lens should be placed on the path of a recording beam. The recording and reference beams were combined through another beam splitter, and the sample was placed at the interferential plane to create in-plane distribution of the photo-alignment molecular axis.

Following by the exposure process, the sample was spin-coated with a reactive mesogen such as RM257 to induce

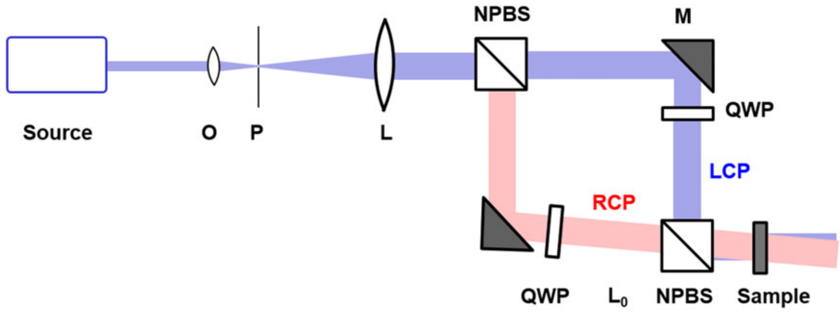

FIGURE 3 — The optical setup for interference exposure of a Pancharatnam–Berry deflector. L, lens; LCP, left-handed circularly polarized light; M, mirror; NPBS, non-polarizing beam splitter; O, objective; P, pin-hole; QWP, quarter-wave plate; RCP, right-handed circularly polarized light.

phase retardation and then UV-cured to solidify the coated reactive mesogen. Multiple coatings might be necessary to ensure high diffractive efficiency.[6,7]

3 Device structure and simulation results

Based on the PBL and PBD described previously, we propose an optical design shown in Fig. 4. The light source, or a light guide plate, generates uniform light output, which is reflected by a polarizing beam splitter toward an LCoS (liquid crystal-on-silicon) panel. The displayed content is then reflected toward a broadband quarter-wave plate to convert the linearly polarized light into circularly polarized light. The PBL stack consists of multiple PBLs with polarization rotators to switch between multiple focusing powers to enable depth content. The total optical power of PBLs is less than three diopters to alleviate longitudinal chromatic aberration caused by its diffractive nature. The light is then passed through PBD due to the polarization selectivity. Upon reflection by the concave mirror, the handedness of the polarization is flipped and then deflected by the PBD into the waveguide. The second PBD is disposed to deflect again and guide light into the viewing region.

Also, based on polarization selectivity, we propose to realize the exit-pupil expansion through polarization management.

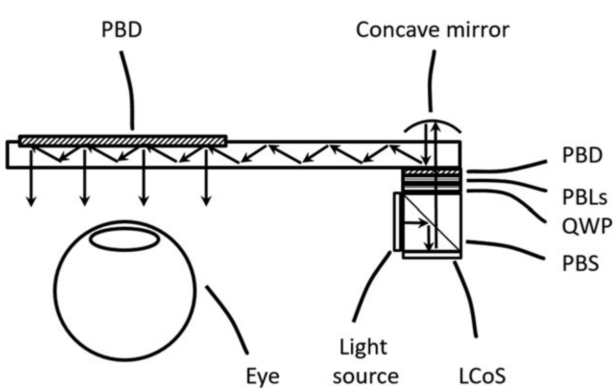

FIGURE 4 — The optical design based on Pancharatnam–Berry lenses (PBLs) and Pancharatnam–Berry deflectors (PBDs). LCoS, liquid crystal-on-silicon; QWP, liquid crystal-on-silicon.

Let us assume an input light of 100% intensity coming from the right side of the waveguide. To obtain uniform output intensity, instead of controlling the diffraction efficiency (η) of the out-coupler (Fig. 5(a)), we propose to control the polarization state as it encounters the PBD out-coupler (Fig. 5(b)). Such a polarization control, instead of efficiency control, allows uniform transmittance of the environment light, and therefore, the device does not show gradient transmittance in appearance. This is achieved by controlling the in-plane crystal axis (azimuthal angle, ϕ) of an liquid crystal (LC) film with fixed thickness t as shown in Fig. 5(b). Because of the maturity of photo-alignment and liquid crystal polymer materials, precise control of LC film thickness and azimuthal angle distribution can be easily achieved.

In Fig. 6, we show the capability of controlling the amount of out-coupling simply by controlling the crystal axis ϕ of a 0.8-μm LC film. At $\phi = 0°$, the out-coupling ratio is over 90%, while at $\phi = 45°$, this ratio is reduced to 0%. Therefore, any intermediate state of out-coupling ratio can be achieved by setting $0° \leq \phi \leq 45°$.

The dependence of output efficiency on the azimuthal angel of LC is explored by means of Finite Difference Frequency Domain simulation method, whose result is shown in Fig. 7. The trend of out-coupling ratio can be roughly matched for three primary colors when ϕ lies between 45° to 70°. In this region, the single-waveguide design can be made possible. Depending on the desired parameters for the size of exit-pupil, different arrangement can be made.

4 Depth adaption based on light field rendering

By defining two arbitrary parallel planes (first plane and second plane) with certain non-zero spacing, the intensity distribution of all light rays can be described as

$$L = L(x, y; u, v), \tag{3}$$

where x and y are the coordinates on the first plane, and u and v are the coordinates on the second plane. The function L is

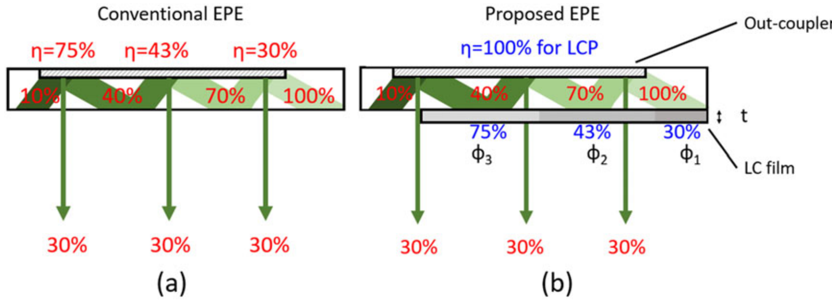

FIGURE 5 — Illustrations of (a) conventional exit-pupil expansion (EPE) and (b) our proposed EPE. LC, Liquid crystal; LCP, left-handed circularly polarized light.

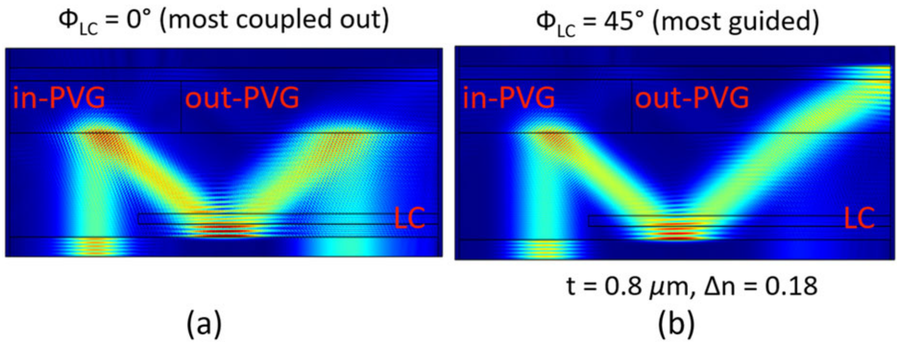

FIGURE 6 — Polarization-based exit-pupil expansion at different LC azimuthal angles: (a) ϕ = 0° and (b) ϕ = 45°. λ_0 = 550 nm.

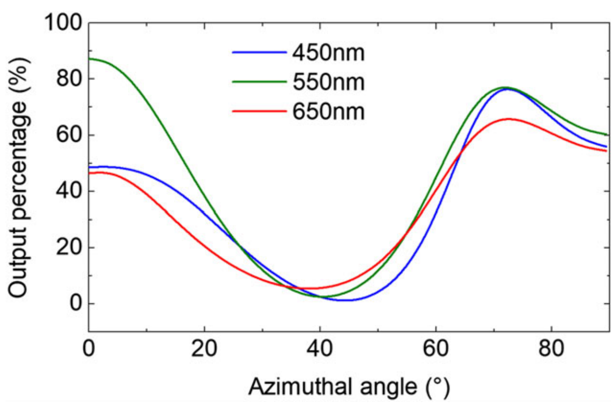

FIGURE 7 — Simulated output percentage of polarization-based exit-pupil expansion at different LC azimuthal angles and red, green and blue wavelengths.

usually referred to as light field. A light field function inherently contains the depth information of an environment. For example, if an observer's eye can move freely on the first plane, then at each point (x, y) on the first plane, the observer sees a different picture (u, v). The parallax from the pictures will reveal how far away each object is. Therefore, if a light field is faithfully reproduced, the depth content is also reproduced. To reproduce a light field, multiple LCD panels/display distances are required. Depending on how the display images on each panel is combined, three different methods can be defined: additive light field,[11,12] multiplicative light field,[13] and polarization light field.[14] In this work, we focus on the additive light field rendering as the other methods are not in the scope.

A multi-focal display can be exploited to reconstruct such light field by assigning computationally generated 2D images to corresponding subframes with different depths. In this demonstration, we only use two depths (i.e., one switchable PBL). Please pay close attention that the first plane and second plane mentioned previously are different from the first and second subframes that will appear repetitively later on.

As shown in Fig. 8, at different subframes, the physical display panel is projected by the PBLs to different depths (referred to as subframes 1 and 2). Because all the display light is from incoherent illumination sources, its intensity, along a specific direction, can be directly superimposed:

$$I_{\text{total}} = I_i + I_j, \tag{4}$$

where I_i and I_j represent the intensity of specific pixels along specific direction from the first and second subframes. To account for all pixels along all directions, we first define the first light field plane as the location of eye box and the second light field plane (reference plane) at an arbitrary distance d_0 away from the eye box. Then, the addition of light rays from subframes can be described as

$$L\left(x_p, y_p, u_r, v_r\right) = \sum_{k=1}^{2} I_k\left(x_p + h_k \frac{u_r}{d_0}, y_p + h_k \frac{v_r}{d_0}\right). \tag{5}$$

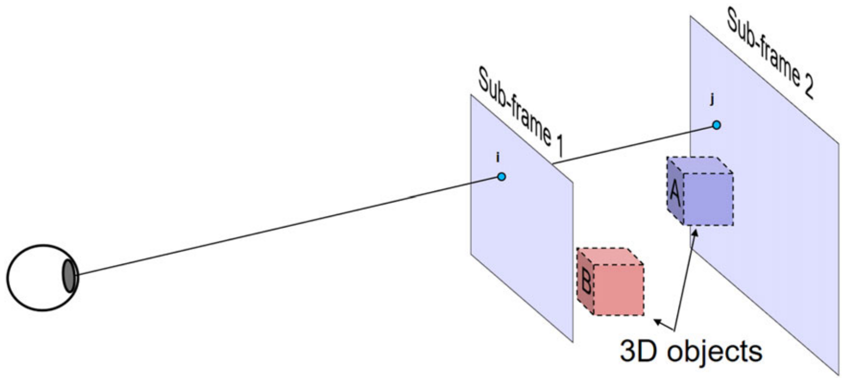

FIGURE 8 — Schematic plot of light field rendering with two subframes. Two 3D objects (A and B blocks) are depicted, illustrating the desired 3D scene when two subframes are combined.

Equation (5) essentially establishes the correlation between two subframes and the combined light field L. For the ease of computation, the first plane is discretized into "view points" covering the eye box, and x_p and y_p denote the coordinates of pth view point; the second plane is discretized into "imaginary pixels on Reference Panel" with u_r and v_r denote the coordinates of rth pixel; I_k is the intensity of the image from the kth subframe, and h_k denotes the depth of kth subframe.

Equation (5) can be rewritten in matrix form by expressing all pixels on subframe in a concatenated column vector $\mathrm{I}_{k,l}$, where k and l refer to the lth pixel on the kth subframe. The imaginary pixels seen from different view points are written in a concatenated column vector $\mathrm{L}_{p,r}$, where p and r refer to the rth pixel seen from the pth view point. L is referred to as the light field vector. The addition relation, Eq. (5), between I and L is expressed as the addition matrix M by sorting out the geometric correlation between the

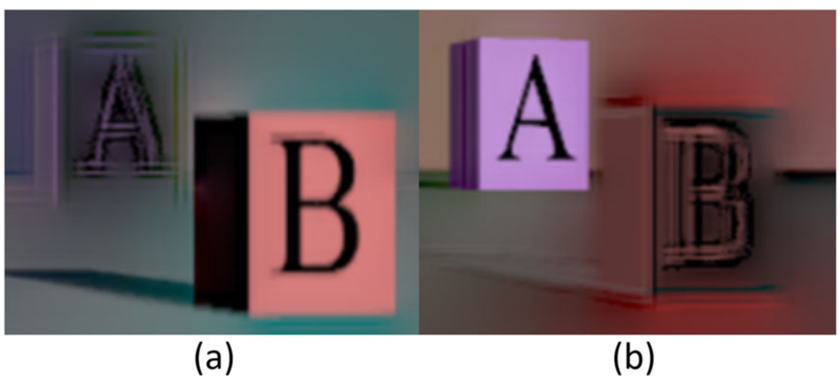

FIGURE 9 — The rendered images for (a) subframe 1 and (b) subframe 2. The fast switching of these two subframes results in an additive-intensity light field, which resembles the designated 3D scene.

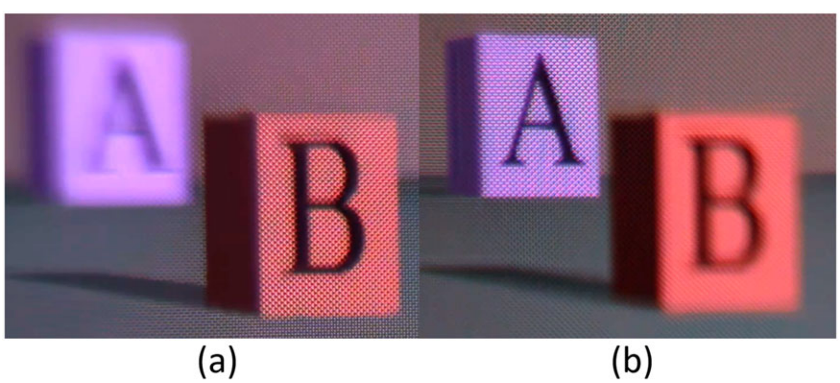

FIGURE 10 — The images seen through the apparatus by a camera focusing at (a) near distance and (b) far distance.

subframe and the reference panel. Then, we can express Eq. (5) in a simple matrix form:

$$\mathbf{L} = \mathbf{MI}. \tag{6}$$

A desired target light field vector, T, is generated by capturing images from different view points in a 3D scene rendered with developed software such as POV-ray™ or 3ds Max™. The displayed images on each subframe can then be determined by minimizing the difference between the added light field vector L and the desired target light field vector T. This can be expressed as an optimization problem:

$$\arg\min_{\mathbf{I}} \|\mathbf{L} - \mathbf{T}\|^2, \mathbf{L} = \mathbf{MI}, \mathbf{T} = \begin{bmatrix} T_1 \\ T_2 \\ \vdots \\ T_N \end{bmatrix}. \tag{7}$$

By solving Eq. (7), the displayed images for the subframes can be determined. In our example, two blocks marked "A" and "B" at a spacing of 0.8 D are used as target 3D scene, and the device is setup to generate a switching of 1 D at 60 Hz video frame rate (i.e., switching on for 1/120 s for subframe 1 and switching off for 1/120 s for subframe 2). With this apparatus, two subframes can reproduce a depth adaption of one diopter. The images generated following Eq. (7) for subframes 1 and 2 are shown in Fig. 9. With a camera shooting through our apparatus, the resultant images were captured and shown in Fig. 10. The image observed this way provides true depth adaption; that is, the user can focus to the near object (Fig. 10(a)) or the far object (Fig. 10(b)) upon choice. This provides monocular depth cue based on eye accommodation and can potentially improve user experience when using a near-eye display.

5 Conclusion

To conclude, a novel design of see-through near-eye display system for augmented reality application is proposed in this work. The input and output coupling PBD simply fabricated by spin-coating and UV exposure can achieve around 100% coupling efficiency. The exit-pupil expansion can be realized through polarization management by pre-designed LC layers instead of gradient efficiency, allowing uniform ambient transmittance. The fast depth adaption of the image can also be achieved through PBLs with appropriate light field rendering. The combined utilization of PBD and PBL allows compact on-axis optical design with depth control of the display content. Although the off-axis performance of this design still has room to be improved, we believe this work will make good impact to see-through near-eye displays.

Acknowledgments

The authors thank Intel and Air Force Office of Scientific Research (AFOSR) (FA9550-14-1-0279) for financial aid during the research period of this work.

References

1 T. Levola and V. Aaltonen, "Near-to-eye display with diffractive exit pupil expander having chevron design," *J. Soc. Inf. Disp.*, **16**, No. 8, 857–862 (2008). https://doi.org/10.1889/1.2966447.

2 P. Äyräs *et al.*, "Exit pupil expander with a large field of view based on diffractive optics," *J. Soc. Inf. Disp.*, **17**, No. 8, 659–664 (2009). https://doi.org/10.1889/JSID17.8.659.

3 S. Pancharatnam, "Generalized theory of interference and its applications," *Proc. Indian Acad. Sci., Sect. A*, **44**, No. 5, 247–262 (1956). https://doi.org/10.1007/BF03046050.

4 M. V. Berry, "Quantal phase factors accompanying adiabatic changes," *Proc. R. Soc. London, Ser. A*, **392**, No. 1802, 45–57 (1984). https://doi.org/10.1098/rspa.1984.0023.

5 C. Oh and M. J. Escuti, "Achromatic diffraction from polarization gratings with high efficiency," *Opt. Lett.*, **33**, No. 20, 2287–2289 (2008). https://doi.org/10.1364/OL.33.002287.

6 K. Gao *et al.*, "High-efficiency large-angle Pancharatnam phase deflector based on dual-twist design," *Opt. Express*, **25**, No. 6, 6283–6293 (2017). https://doi.org/10.1364/OE.25.006283.

7 Y. H. Lee *et al.*, "Reflective polarization volume gratings for high efficiency waveguide-coupling augmented reality displays," *Opt. Express*, **25**, No. 22, 27008–27014 (2017). https://doi.org/10.1364/OE.25.027008.

8 Y. H. Lee *et al.*, "Recent progress in Pancharatnam–Berry phase optical elements and the applications for virtual/augmented realities," *Optical Data Process. Storage*, **3**, No. 1, 79–88 (2017). https://doi.org/10.1515/odps-2017-0010.

9 J. Kim *et al.*, "Fabrication of ideal geometric-phase holograms with arbitrary wavefronts," *Optica*, **2**, No. 11, 958–964 (2015). https://doi.org/10.1364/OPTICA.2.000958.

10 J. Wang *et al.*, "Effects of humidity and surface on photoalignment of brilliant yellow," *Liq. Cryst.*, **44**, No. 5, 863–872 (2017). https://doi.org/10.1080/02678292.2016.1247479.

11 S. Lee *et al.*, "Additive light field displays: realization of augmented reality with holographic optical elements," *ACM Trans. Graph.*, **35**, No. 4, 60–13 (2016). https://doi.org/10.1145/2897824.2925971.

12 T. Zhan *et al.*, "High-resolution additive light field near-eye display by switchable Pancharatnam–Berry phase lenses," *Opt. Express*, **26**, No. 4, 4863–4872 (2018). https://doi.org/10.1364/OE.26.004863.

13 F. C. Huang *et al.*, "The light field stereoscope: immersive computer graphics via factored near-eye light field displays with focus cues," *ACM Trans. Graph.*, **34**, No. 4, 60–60:12 (2015). https://doi.org/10.1145/2766922.

14 D. Lanman *et al.*, "Polarization fields: dynamic light field display using multi-layer LCDs," *ACM Trans. Graph*, **30**, No. 6, 186 (2011). https://doi.org/10.1145/2070781.2024220.

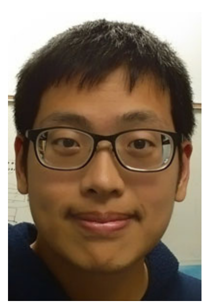

Yun-Han Lee received a BS degree in Physics from the National Central University (Taiwan) in 2011 and MS degree in Physics from the National Taiwan University in 2013 and is currently working toward a PhD degree from the College of Optics and Photonics, University of Central Florida, Orlando. His current research interests include fast phase modulators and near-eye displays including augmented reality and virtual reality displays.

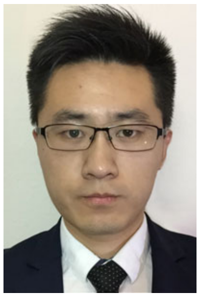

Guanjun Tan received a BS degree in Physics from the University of Science and Technology of China in 2010 and is currently working toward a PhD degree from the College of Optics and Photonics, University of Central Florida, Orlando. His current research interests include OLEDs, QLEDs, and novel liquid crystal display technologies.

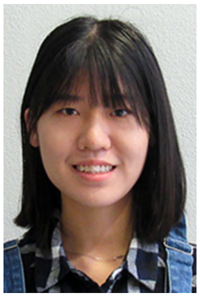

Kun Yin received a BS in Opto-Electronics, School of Precision Instrument and Opto-Electronics Engineering, Tianjin University (China) and is currently working toward a PhD degree from the College of Optics and Photonics, University of Central Florida, Orlando. Her current research interests include optical gratings and augmented reality and virtual reality displays.

Tao Zhan received a BS degree in Physics from Nanjing University in 2016 and is currently working toward a PhD degree from the College of Optics and Photonics, University of Central Florida, Orlando. His current research interests include light field displays, near-eye displays, and novel liquid crystal devices.

Shin-Tson Wu is Pegasus Professor at the College of Optics and Photonics, University of Central Florida. He is among the first six inductees of the Florida Inventors Hall of Fame (2014) and a Charter Fellow of the National Academy of Inventors (2012). He is a Fellow of the IEEE, OSA, SID, and SPIE and an honorary Professor at Nanjing University (2013) and at National Chiao Tung University (2017). He is the recipient of 2014 OSA Esther Hoffman Beller Medal, 2011 SID Slottow-Owaki Prize, 2010 OSA Joseph Fraunhofer Award, 2008 SPIE G. G. Stokes Award, and 2008 SID Jan Rajchman Prize. Presently, he is serving as SID honors and awards committee chair.